PHYSICAL REVIEW B **96**, 161201(R) (2017)

Four-phonon scattering significantly reduces intrinsic thermal conductivity of solids

Tianli Feng,[1] Lucas Lindsay,[2] and Xiulin Ruan[1,*]

[1]*School of Mechanical Engineering and the Birck Nanotechnology Center, Purdue University, West Lafayette, Indiana 47907-2088, USA*

[2]*Materials Science and Technology Division, Oak Ridge National Laboratory, Oak Ridge, Tennessee 37831, USA*

(Received 26 April 2017; published 27 October 2017)

For decades, the three-phonon scattering process has been considered to govern thermal transport in solids, while the role of higher-order four-phonon scattering has been persistently unclear and so ignored. However, recent quantitative calculations of three-phonon scattering have often shown a significant overestimation of thermal conductivity as compared to experimental values. In this Rapid Communication we show that four-phonon scattering is generally important in solids and can remedy such discrepancies. For silicon and diamond, the predicted thermal conductivity is reduced by 30% at 1000 K after including four-phonon scattering, bringing predictions in excellent agreement with measurements. For the projected ultrahigh-thermal conductivity material, zinc-blende BAs, a competitor of diamond as a heat sink material, four-phonon scattering is found to be strikingly strong as three-phonon processes have an extremely limited phase space for scattering. The four-phonon scattering reduces the predicted thermal conductivity from 2200 to 1400 W/m K at room temperature. The reduction at 1000 K is 60%. We also find that optical phonon scattering rates are largely affected, being important in applications such as phonon bottlenecks in equilibrating electronic excitations. Recognizing that four-phonon scattering is expensive to calculate, in the end we provide some guidelines on how to quickly assess the significance of four-phonon scattering, based on energy surface anharmonicity and the scattering phase space. Our work clears the decades-long fundamental question of the significance of higher-order scattering, and points out ways to improve thermoelectrics, thermal barrier coatings, nuclear materials, and radiative heat transfer.

DOI: 10.1103/PhysRevB.96.161201

Phonons are quasiparticles that quantize lattice vibrations. They interact with each other through scattering events, with the most significant scattering processes known as three-phonon processes. Recently, thermal conductivity (κ) calculations based on density functional theory have found incredible agreement with measured κ values for a variety of systems and made striking predictions of thermal processes despite considering only lowest-order perturbative intrinsic scattering from three-phonon interactions [1–4]. However, a persistent fundamental question for decades has been the following: What is the impact of four-phonon and higher-order scattering? Due to the lack of formalism and computational power, four-phonon scattering has been ignored in previous studies. However, this question has become particularly relevant, since first-principles methods have overestimated the measured thermal conductivities of a number of materials [2,3,5–7]. For example, while some predictions give reasonable accuracy with measured data at low temperatures, they overpredict significantly at higher temperatures, diminishing the predictive power for applications such as thermal barrier coatings and high-temperature thermoelectrics [2]. Moreover, such deviations can become quite large even at room temperature (RT) for some technologically important materials such as c-BN [3,5] and SnSe [6,7]. As an example for thermal management applications, Lindsay *et al.* have predicted that the zinc-blende structure, boron arsenide (BAs), may have a thermal conductivity ~2200 W/m K at room temperature, higher than the known best heat conductor, diamond [3]. This might open new opportunities for passive cooling and other thermal management applications. The BAs system has been synthesized, however, the measured thermal conductivity has only reached ~200 W/m K. [8,9]. Extrinsic defects and grain boundaries are possible causes for this discrepancy, or higher-order intrinsic scattering may become significant in determining the upper limit of k in this material.

The prediction of four-phonon scattering has been pursued for a long time. Lindsay *et al.* examined the phase space for four-phonon scattering processes [10]. Turney *et al.* studied the fourth- and higher-order anharmonicity of the interatomic potential of argon, by truncating the potential in molecular dynamics (MD) simulations [11]. Sapna and Singh estimated the four-phonon scattering rates in carbon nanotubes using an analytical model involving approximations such as the Callaway model, the Debye model, etc. [12]. Despite those efforts, a direct and rigorous calculation of four-phonon scattering rates was not available until recently [13]. However, the anharmonic force constants therein were obtained from classical force fields, and thus the results are only qualitative and cannot be validated against experiments. In this Rapid Communication, we have calculated four-phonon scattering rates fully from first principles and examined their impact on the thermal conductivity and optical phonon lifetimes of BAs, Si, and diamond. We demonstrate that four-phonon scattering resistance can reduce their predicted thermal conductivities and optical phonon lifetimes significantly, manifesting the general impact of four-phonon scattering in solids.

Intrinsic phonon scattering is caused by lattice anharmonicity [14]. From perturbation theory, the lowest-order anharmonic couplings involve three phonons: A single phonon may split into two phonons, or two phonons may combine to create a new phonon, as shown in Fig. 1(a). In addition to these scatterings, second-order anharmonicity gives rise to four-phonon processes given in Fig. 1(b). The three- and four-phonon scattering rates for each phonon mode are calculated by summing up the probabilities of all possible scattering

*ruan@purdue.edu

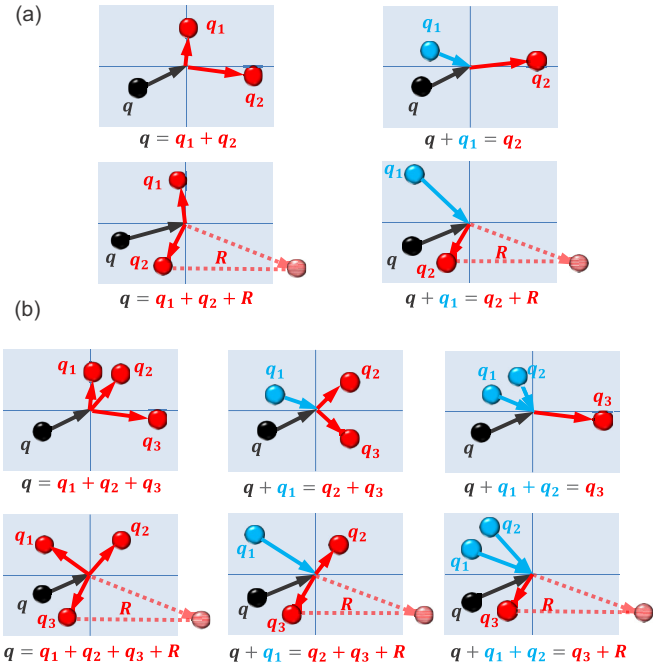

FIG. 1. Three- and four-phonon scattering diagrams. (a) Three-phonon splitting and combination processes. (b) Four-phonon splitting, redistribution, and combination processes. The shaded rectangles represent the first Brillouin zone (BZ). The phonon momentum is $\hbar\mathbf{q}$ with $\mathbf{q}$ standing for wave vector. The processes with momentum conserved are normal processes. The others with momentum nonconserved are umklapp processes, in which the resulting phonons are folded back by reciprocal lattice vectors $\mathbf{R}$.

events involving this mode. Each transition probability is calculated by Fermi's golden rule from density functional theory [13]. The computational cost is very high but can be mitigated as described in our earlier work [13]. See the Methods and Computational Challenge sections in the Supplemental Material [15].

We have obtained the scattering rates for each of the 24 576 (870 irreducible) phonon modes in the first BZ discretized by a $16 \times 16 \times 16$ $\mathbf{q}$ mesh from 10 to 1300 K for BAs, Si, and diamond. The results as a function of phonon frequency at 300 and 1000 K are shown in Figs. 2(a)–2(f). The insets show the low-frequency behavior. Contradictory to the prevailing general notion that four-phonon scattering is negligible, we find that for many frequencies the four-phonon scattering is comparable to or even much stronger than the lower-order three-phonon scattering, as highlighted by the blue ovals.

Most surprisingly, the four-phonon scattering in BAs is quite strong, as shown in Fig. 2(a). This behaves against the general notion of perturbation theory, in which the strength of four-phonon scattering is driven by the magnitude of higher-order terms of the Hamiltonian, which are small in BAs. The origin of the strong four-phonon scattering in BAs is illustrated in Fig. 3(a). As shown in Ref. [3], the number of three-phonon processes is partly restricted by a large acoustic-optical (a-o) energy gap, which prevents two acoustic phonons from combining into an optical phonon as well as the reverse process since the summation of the energies of two acoustic phonons cannot reach that of the optical phonon. This coupling with closely bunched acoustic branches contributes to weak three-phonon scattering and the predicted ultrahigh-thermal conductivity in BAs [3]. Further evidence of this can be found near 21 THz in Fig. 2(a), in which the three-phonon scattering rates have a deep valley. These phonons are the optical modes near the Γ point and have high energies and small momentums. They can hardly find two other phonon modes that satisfy energy conservation and momentum conservation simultaneously. Such a large a-o gap, however, does not forbid four-phonon processes between acoustic and optical phonons. For example, at around 21 THz, the possible number of three-phonon scattering configurations is smaller than 20 while the number of four-phonon processes is about 10^7–10^8. For these four-phonon processes, 94% are $\mathbf{q} + \mathbf{q}_1 \rightarrow \mathbf{q}_2 + \mathbf{q}_3$ and 6% are $\mathbf{q} \rightarrow \mathbf{q}_1 + \mathbf{q}_2 + \mathbf{q}_3$. Therefore, the optical phonon relaxation time is brutally overpredicted by the three-phonon picture. When the four-phonon term is included, the relaxation time is reduced from 10^4 to 40 ps at room temperature (see Supplemental Fig. S1 [15]). Since these optical phonons near the Γ point are critical for interactions with electrons and photons such as in laser heating [16] and for infrared optical properties [17], the long lifetime predicted from three-phonon scattering is misleading, while four-phonon scattering is critical and should be included.

As temperature increases to 1000 K, the four-phonon scattering of BAs becomes much more important, especially for phonons with higher frequencies, as highlighted by the blue ovals in Fig. 2(b). The variations with temperature and frequencies are shown in Figs. 3(b) and 3(c), from which we determine the scaling law of four-phonon scattering $\tau_4^{-1} \sim T^2\omega^4$. Compared to three-phonon scattering, four-phonon scattering is more important at higher temperatures and for higher-energy phonons as the phonon population increases with temperature and the phase space increases with phonon energy (frequency). Due to their simplicity, scaling laws are of great importance in thermal nanoengineering as well. For example, the power law of three-phonon scattering $\tau_3^{-1} \sim T\omega^2$ and phonon-defect scattering $\tau_d^{-1} \sim \omega^4$ has been widely used in understanding the experimental thermal conductivity in advanced thermoelectric materials [18,19].

In the other two materials without phonon band gaps, Si and diamond, four-phonon scattering is not as strong as in BAs but certainly not negligible. At 300 K, τ_4^{-1} is well below τ_3^{-1} for most of the acoustic phonons. This obeys the general notion in perturbation theory since the anharmonicity (the higher-order terms of the Hamiltonian) is small for Si and diamond. Nevertheless, the optical modes marked by the blue ovals still have large four-phonon rates, and this may explain why calculated infrared optical linewidths considering only three-phonon scattering are narrower than experiments [17,20]. As T increases to 1000 K, four-phonon rates of the low-frequency phonons remain insubstantial, however, higher-energy longitudinal acoustic (LA) modes and all the optical modes exhibit large τ_4^{-1}, comparable to τ_3^{-1}. The large τ_4^{-1} of the heat-carrying LA phonons will have a substantial effect on the thermal conductivity of these materials. In all the materials we note that the low-frequency limits for both three- and four-phonon scatterings obey the law $\lim_{\omega\rightarrow 0} \tau^{-1} = 0$ resulting from translational invariance, indicating the accuracy

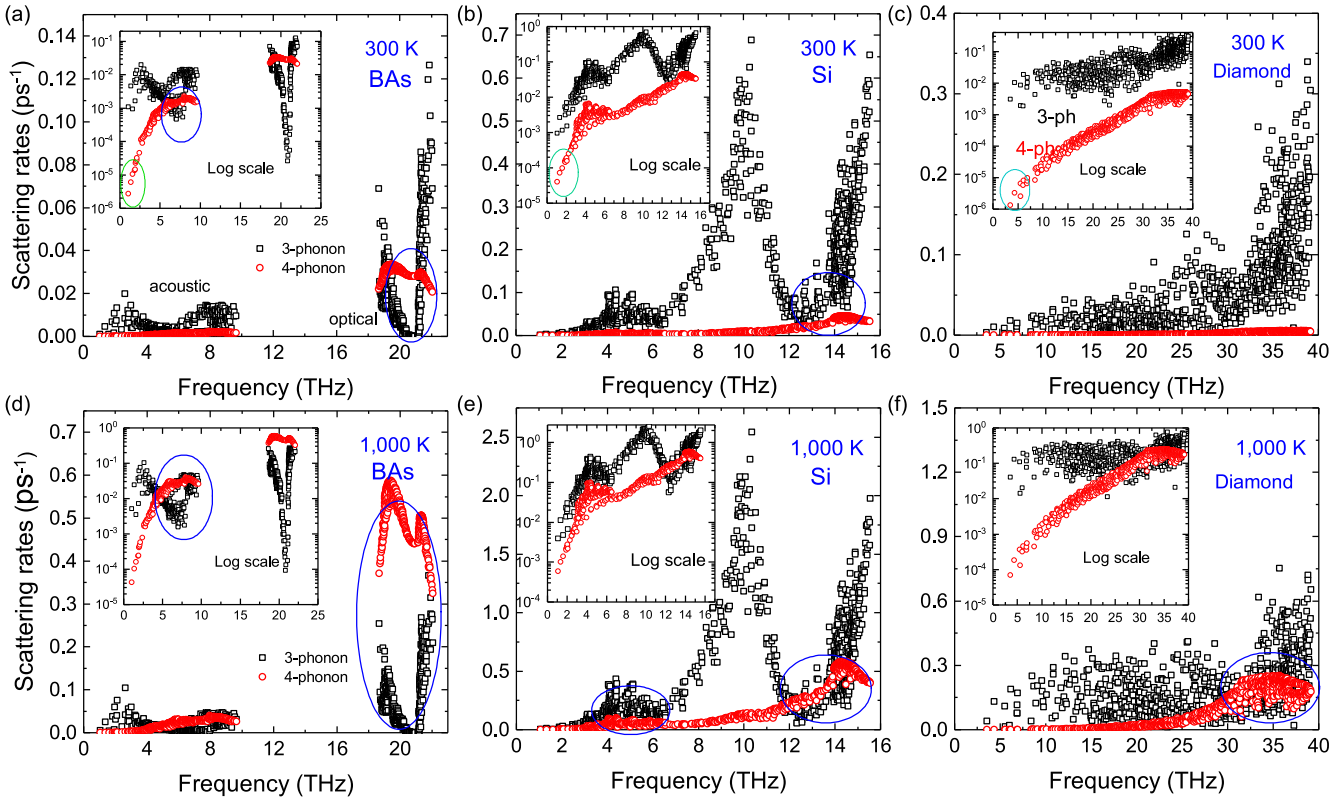

FIG. 2. First-principles three-phonon (black dots) and four-phonon (red dots) scattering rates of BAs, Si, and diamond at 300 and 1000 K. The insets are in log-linear scales to give a better view of the low-frequency regions. Blue ovals indicate the regions where four-phonon scattering plays an important role. Green ovals in the insets indicate that our four-phonon results reproduce well the universal law $\lim_{\omega\to 0}\tau^{-1}=0$, which is a critical mark of the calculation accuracy.

of our four-phonon calculations. The same as that in BAs, the power-law fittings for diamond and silicon give $\tau_4^{-1}\sim\omega^4$, which are shown in Supplemental Fig. S2 [15].

We have also calculated κ beyond the relaxation time approximation (RTA) by exactly solving the phonon Boltzmann transport equation (BTE) using an iterative scheme mixing three-phonon interactions [1,3]. In this work, due to the high computational cost, the four-phonon scattering rates are computed at the RTA level only and inserted into the iterative scheme that determines the nonequilibrium phonon distributions from mixing of the three-phonon processes. This is similar to employing phonon-isotope and phonon-boundary scattering terms in the full BTE solution [1,21]. We will show that such an approximation is likely valid as four-phonon

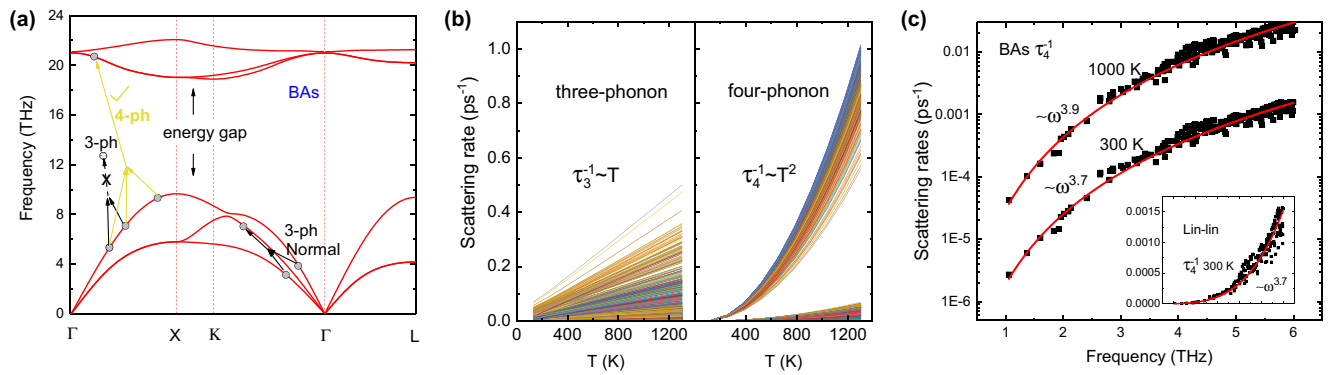

FIG. 3. Impacts of phonon band gap, temperature, and frequency on three- and four-phonon scattering. (a) Three- and four-phonon processes in BAs. The large energy gap between acoustic and optical phonons forbids three-phonon processes, however, it is not as restrictive for four-phonon processes. The three-phonon process is dominated by intraband normal scattering, while the four-phonon process is dominated by inner and interband umklapp scattering. (b) Temperature dependencies of three-phonon and four-phonon scatterings of BAs. The curves cover all the modes in the BZ, with each curve corresponding to a different mode. (c) Power-law fitting $\tau_4^{-1}=A\omega^\eta$ of the acoustic phonons in BAs. The log-linear scale gives a clear view of the low-frequency behavior, while the inserted linear-linear scale is for the view of the high-frequency behavior.

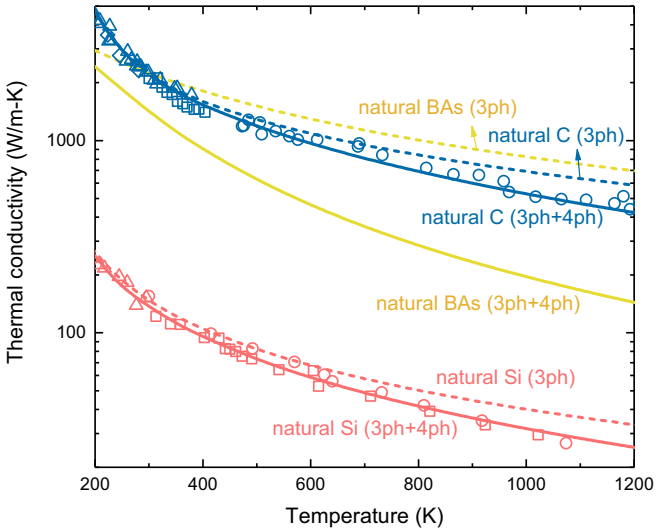

FIG. 4. Thermal conductivities of naturally occurring BAs, Si, and diamond. Dashed lines give calculated κ_3, while solid lines give κ_{3+4}. Note that these calculations employed the iterative solution of the BTE, beyond the RTA. Symbols represent measured data: red triangles [23], red squares [24], red circles [25], blue triangles [26], blue squares [27], blue circles [28], and blue diamonds [29]. No experimental data are available for single-crystal BAs.

scattering is dominated by umklapp processes. We also include phonon-isotope scattering [22] in these κ calculations of naturally occurring materials.

The thermal conductivities κ of the naturally occurring materials are shown in Fig. 4. For diamond and Si the three-phonon predictions agree well with measured data at low temperature (<600 K for Si, <900 K for diamond), however, significant deviations from experiment occur at high temperatures. For example, at 1000 K, three-phonon scattering alone overpredicts κ of diamond and silicon by 31% and 26% as compared to experimental values, respectively. After including four-phonon scattering, we find that the predicted thermal conductivity agrees well with measurements throughout the entire temperature range. Such a reduction is beneficial for thermoelectrics and thermal barrier coatings where low thermal conductivities are desired. As for naturally occurring BAs, even at room temperature, the thermal conductivity is reduced significantly, from 2241 to 1417 W/m K, after including four-phonon scattering. As temperature increases to 1000 K, the reduction grows to over 60%. Nonetheless, the room-temperature intrinsic thermal conductivity of BAs is still among the highest of known materials, and much higher than common metals. Moreover, the well-known temperature scaling $\kappa \sim 1/T$ at high temperatures by only considering three-phonon scattering can now be modified to $\kappa \sim 1/(AT + BT^2)$ after adding four-phonon scattering.

Here, we discuss important physical details regarding four-phonon scattering processes. More discussions on computational details can be found in the Supplemental Material, i.e., the impact of broadening factors, $\mathbf{q}$ meshes, interatomic cutoff radius, translational invariance, force constant truncation, and the role of normal and umklapp processes [15].

TABLE I. Anharmonicity ratio $|\Phi_4/\Phi_3|^2/|\Phi_2|$ to approximate the relative importance of four-phonon scattering in diamond, Si, BAs, and CuCl. Units of the representative nth-order force constant are eV/Å^n. The representative force constant values are taken at $\Phi_{0,0,x,x}$, $\Phi_{0,0,0,x,y,z}$, and $\Phi_{0,0,0,0,x,x,x,x}$. The index 0 indicates the origin primitive cell (see the Supplemental Material for more details [15]). The third-order $\Phi_{0,0,0,x,x,x} = 0$ due to symmetries cannot be taken as the anharmonicity.

Material	Atom	$\lvert\Phi_2\rvert$	$\lvert\Phi_3\rvert$	$\lvert\Phi_4\rvert$	$\lvert\Phi_4/\Phi_3\rvert^2/\lvert\Phi_2\rvert$
Diamond	C	44.2	95.0	224	0.128
BAs	B	17.0	45.6	65.7	0.122
Si	Si	13.6	33.9	50.8	0.165
CuCl	Cu	1.93	13.1	48.0	6.956

Estimating the significance of four-phonon scattering. As discussed above, four-phonon scattering becomes increasingly important at higher temperatures in all materials; however, after careful examination of the three materials in this work, a natural question is as follows: How important is four-phonon scattering generally in other solids? As with three-phonon scattering, four-phonon scattering is governed by two factors, anharmonicity of the energy surface and the scattering phase space. We note that the construction of both three- and four-phonon scattering rates is nontrivial, each a complex interplay of matrix elements, eigenvectors, and frequencies combining various phonon modes. However, based on the phonon scattering formalism [13], we attempt to estimate the relative importance of the fourth-order anharmonicity. Yue *et al.* have done some estimations by evaluating the fourth-order terms in Hamiltonians [30]. Roughly speaking, the nth-order phonon scattering rate is proportional to $\tau_n^{-1} \sim |V_n|^2 f^{n-2}/\omega^{n+1}$, where V_n is the nth-order transition matrix element $\sim \Phi_n/m^{n/2}$. Φ_n is the nth-order force constant, m is the average atomic mass, and f is the Bose-Einstein distribution approximated as $\sim k_B T/\hbar\omega$, high-temperature behavior. Approximating the frequency as $\omega \sim \sqrt{\Phi_2/m}$, we get $\tau_n^{-1} \sim |\Phi_n|^2 \sqrt{m} T^{n-2}/|\Phi_2|^{n-1/2}$. Thus, the relative importance of the nth-order anharmonicity to the third-order anharmonicity is crudely evaluated as $\tau_n^{-1}/\tau_3^{-1} \sim |\Phi_n/\Phi_3|^2 T^{n-3}/|\Phi_2|^{n-3}$. Note that this captures the increasing importance of higher-order scattering with increasing temperature and only requires single calculations of a second-, third-, and higher-order derivative of the potential energy.

Table I gives the relative strength of the fourth-order anharmonicity ($|\Phi_4/\Phi_3|^2/|\Phi_2|$) for the materials studied in this work and a low thermal conductivity zinc-blende material, CuCl (~1 W/m K at room temperature) [31,32]. Note that the temperature dependence is omitted. This simplistic formalism is intended to give a rough estimation for when higher-order scattering may be important in one material over another. As shown in Table I, the fourth-order anharmonicity is predicted to be significantly more important in CuCl than in the high conductivity materials considered here. Our previous work based on interatomic potentials directly demonstrated a positive correlation between four-phonon scattering and anharmonicity [13]. In soft materials, such as those of interest for thermoelectric and thermal barrier coating applications [4], atoms can deviate significantly from

equilibrium to sample higher anharmonicity, and fourth-order terms in their Hamiltonians can be quite large [30]. Note that $|\Phi_4/\Phi_3|^2/|\Phi_2|$ is higher in Si than in diamond, and Si also has fourth-order scattering that is relatively more important.

This simple formalism, however, does not account for the phase space for three- and four-phonon scattering processes. Thus, even though the fourth-order anharmonicity is predicted to be relatively less important in BAs as demonstrated in Table I, the BAs conductivity is still significantly reduced by four-phonon scattering resistance (Fig. 4). In materials where three-phonon scattering is weak due to dispersion features (e.g., phonon band gap, acoustic bunching [3]) that reduce the phase space, we expect four-phonon scattering to also be important, for instance, in BSb [3] and BeSe [33].

In summary, we have rigorously calculated four-phonon scattering rates and thermal resistance from fully first-principles methods. Due to the large number of possible scattering configurations, four-phonon processes play an important role in determining intrinsic phonon transport. We find that four-phonon scattering is surprisingly strong in zinc-blende BAs, and reduces its thermal conductivity substantially from ∼2200 to ∼1400 W/m K even at room temperature when compared to previous calculations. The room-temperature optical phonon lifetime is reduced from 10^4 to 40 ps. These impacts increase substantially with increasing temperature. Such strong four-phonon scattering in BAs originates from weak three-phonon scattering that arises from properties of its phonon dispersion coupled with fundamental conservation conditions. These conditions do not as strictly restrict the available scatterings for four-phonon process. With four-phonon scattering included, the predicted thermal conductivities of silicon and diamond reduce κ by ∼30% at high temperatures, and bring the prediction in agreement with measured data throughout the entire temperature range considered. Based on our findings of the general and significant impact of four-phonon processes on thermal transport and optic mode lifetimes, we expect future predictions of these properties will incorporate this important scattering mechanism, especially when considering engineering materials for energy transfer, conversion, and storage applications.

The work on silicon is supported by the Defense Advanced Research Projects Agency (Award No. HR0011-15-2-0037), and the work on diamond and boron arsenide is supported by the National Science Foundation (Award No. 1150948). L.L. acknowledges support from the U.S. Department of Energy, Office of Science, Office of Basic Energy Sciences, Materials Sciences and Engineering Division.

[1] D. A. Broido, M. Malorny, G. Birner, N. Mingo, and D. A. Stewart, Appl. Phys. Lett. **91**, 231922 (2007).

[2] K. Esfarjani, G. Chen, and H. T. Stokes, Phys. Rev. B **84**, 085204 (2011).

[3] L. Lindsay, D. A. Broido, and T. L. Reinecke, Phys. Rev. Lett. **111**, 025901 (2013).

[4] A. Seko, A. Togo, H. Hayashi, K. Tsuda, L. Chaput, and I. Tanaka, Phys. Rev. Lett. **115**, 205901 (2015).

[5] M. Novikov, T. Ositinskaya, O. Shulzhenko, O. Podoba, O. Sokolov, and I. Petrusha, Dopov. Akad. Nauk Ukr. RSR, Ser. A: Fiz.-Mat. Tekh. Nauki **10**, 72 (1983).

[6] L.-D. Zhao, S.-H. Lo, Y. Zhang, H. Sun, G. Tan, C. Uher, C. Wolverton, V. P. Dravid, and M. G. Kanatzidis, Nature (London) **508**, 373 (2014).

[7] R. Guo, X. Wang, Y. Kuang, and B. Huang, Phys. Rev. B **92**, 115202 (2015).

[8] H. Ma, C. Li, S. Tang, J. Yan, A. Alatas, L. Lindsay, B. C. Sales, and Z. Tian, Phys. Rev. B **94**, 220303 (2016).

[9] J. Kim, D. A. Evans, D. P. Sellan, O. M. Williams, E. Ou, A. H. Cowley, and L. Shi, Appl. Phys. Lett. **108**, 201905 (2016).

[10] L. Lindsay and D. A. Broido, J. Phys.: Condens. Matter **20**, 165209 (2008).

[11] J. E. Turney, E. S. Landry, A. J. H McGaughey, and C. H. Amon, Phys. Rev. B **79**, 064301 (2009).

[12] P. Sapna and T. J. Singh, Mod. Phys. Lett. B **27**, 1350117 (2013).

[13] T. Feng and X. Ruan, Phys. Rev. B **93**, 045202 (2016).

[14] A. Maradudin and A. Fein, Phys. Rev. **128**, 2589 (1962).

[15] See Supplemental Material at http://link.aps.org/supplemental/10.1103/PhysRevB.96.161201 for the methods and computational challenge, the relaxation time of the optical phonon at the Γ point in BAs, the power-law fittings for diamond and silicon, the impact of broadening factors, **q** meshes, interatomic cutoff radius, translational invariance, force constant truncation, and the role of normal and umklapp processes.

[16] A. K. Vallabhaneni, D. Singh, H. Bao, J. Murthy, and X. Ruan, Phys. Rev. B **93**, 125432 (2016).

[17] H. Bao, B. Qiu, Y. Zhang, and X. Ruan, J. Quant. Spectrosc. Radiat. Transfer **113**, 1683 (2012).

[18] S. I. Kim, K. H. Lee, H. A. Mun, H. S. Kim, S. W. Hwang, J. W. Roh, D. J. Yang, W. H. Shin, X. S. Li, Y. H. Lee *et al.*, Science **348**, 109 (2015).

[19] M. Hong, T. C. Chasapis, Z.-G. Chen, L. Yang, M. G. Kanatzidis, G. J. Snyder, and J. Zou, ACS Nano **10**, 4719 (2016).

[20] A. Debernardi, Phys. Rev. B **57**, 12847 (1998).

[21] L. Lindsay, D. A. Broido, and N. Mingo, Phys. Rev. B **80**, 125407 (2009).

[22] S.-i. Tamura, Phys. Rev. B **27**, 858 (1983).

[23] T. Ruf, R. Henn, M. Asen-Palmer, E. Gmelin, M. Cardona, H.-J. Pohl, G. Devyatych, and P. Sennikov, Solid State Commun. **115**, 243 (2000).

[24] B. Abeles, D. Beers, G. Cody, and J. Dismukes, Phys. Rev. **125**, 44 (1962).

[25] C. J. Glassbrenner and G. A. Slack, Phys. Rev. **134**, A1058 (1964).

[26] L. Wei, P. K. Kuo, R. L. Thomas, T. R. Anthony, and W. F. Banholzer, Phys. Rev. Lett. **70**, 3764 (1993).

[27] D. G. Onn, A. Witek, Y. Z. Qiu, T. R. Anthony, and W. F. Banholzer, Phys. Rev. Lett. **68**, 2806 (1992).

[28] J. R. Olson, R. O. Pohl, J. W. Vandersande, A. Zoltan, T. R. Anthony, and W. F. Banholzer, Phys. Rev. B **47**, 14850 (1993).

[29] R. Berman, P. R. W. Hudson, and M. Martinez, J. Phys. C **8**, L430 (1975).

[30] S.-Y. Yue, X. Zhang, G. Qin, S. R. Phillpot, and M. Hu, Phys. Rev. B **95**, 195203 (2017).

[31] G. A. Slack and P. Andersson, Phys. Rev. B **26**, 1873 (1982).

[32] S. Mukhopadhyay, D. Bansal, O. Delaire, D. Perrodin, E. Bourret-Courchesne, D. J. Singh, and L. Lindsay, Phys. Rev. B **96**, 100301 (2017).

[33] L. Lindsay, D. A. Broido, and T. L. Reinecke, Phys. Rev. B **88**, 144306 (2013).

Supplemental Information

Four-phonon scattering significantly reduces intrinsic thermal conductivity of solids

Tianli Feng,[1] Lucas Lindsay,[2] and Xiulin Ruan[1,*]

[1]*School of Mechanical Engineering and the Birck Nanotechnology Center, Purdue University, West Lafayette, Indiana 47907-2088, USA*

[2]*Materials Science and Technology Division, Oak Ridge National Laboratory, Oak Ridge, Tennessee 37831, USA*

(Dated: October 6, 2017)

Methods

Fermi's golden rule

The three- and four-phonon scattering rates are calculated by the summations of the probabilities of all the possible scattering events calculated by Fermi's golden rule (FGR) from density functional theory (DFT):

$$\tau_{3,\lambda,\mathrm{RTA}}^{-1}=\sum_{\lambda_1\lambda_2}\left[\frac{1}{2}(1+n_{\lambda_1}^0+n_{\lambda_2}^0)\mathcal{L}_-+(n_{\lambda_1}^0-n_{\lambda_2}^0)\mathcal{L}_+\right]. \tag{S.1}$$

$$\tau_{4,\lambda,\mathrm{RTA}}^{-1}=\sum_{\lambda_1\lambda_2\lambda_3}\left[\frac{1}{6}\frac{n_{\lambda_1}^0 n_{\lambda_2}^0 n_{\lambda_3}^0}{n_\lambda^0}\mathcal{L}_{--}+\frac{1}{2}\frac{(1+n_{\lambda_1}^0)n_{\lambda_2}^0 n_{\lambda_3}^0}{n_\lambda^0}\mathcal{L}_{+-}+\frac{1}{2}\frac{(1+n_{\lambda_1}^0)(1+n_{\lambda_2}^0)n_{\lambda_3}^0}{n_\lambda^0}\mathcal{L}_{++}\right]. \tag{S.2}$$

Here λ stands for $(\mathbf{q},j)$ with $\mathbf{q}$ and j labeling the phonon wave vector and dispersion branch, respectively. $n^0=(e^{\hbar\omega/k_BT}-1)^{-1}$ is the phonon occupation number, and ω is the phonon angular frequency. The transition probability matrix $\mathcal{L}$ is determined by the third-order and fourth-order interatomic force constants (IFCs)[1].

The expressions for $\mathcal{L}_\pm$ and $\mathcal{L}_{\pm\pm}$ are given by FGR,

$$\mathcal{L}_\pm = 18*2\frac{2\pi}{\hbar}\left|H^{(3)}_{\lambda\lambda_1\lambda_2}\right|^2\delta(E_i-E_f) \tag{S.3}$$

$$= \frac{\pi\hbar}{4N_{\mathbf{q}}}\left|V_\pm^{(3)}\right|^2\Delta_\pm\frac{\delta(\omega_\lambda\pm\omega_{\lambda_1}-\omega_{\lambda_2})}{\omega_\lambda\omega_{\lambda_1}\omega_{\lambda_2}}, \tag{S.4}$$

$$\mathcal{L}_{\pm\pm} = 96*2\frac{2\pi}{\hbar}\left|H^{(4)}_{\lambda\lambda_1\lambda_2\lambda_3}\right|^2\delta(E_i-E_f) \tag{S.5}$$

$$= \frac{\pi\hbar}{4N}\frac{\hbar}{2N_{\mathbf{q}}}\left|V_{\pm\pm}^{(4)}\right|^2\Delta_{\pm\pm}\frac{\delta(\omega_\lambda\pm\omega_{\lambda_1}\pm\omega_{\lambda_2}-\omega_{\lambda_3})}{\omega_\lambda\omega_{\lambda_1}\omega_{\lambda_2}\omega_{\lambda_3}}, \tag{S.6}$$

where $V_\pm^{(3)}$ and $V_{\pm\pm}^{(4)}$ are

$$V_\pm^{(3)}=\sum_{b,l_1b_1,l_2b_2}\sum_{\alpha\alpha_1\alpha_2}\Phi^{\alpha\alpha_1\alpha_2}_{0b,l_1b_1,l_2b_2}\frac{e^{\lambda}_{\alpha b}e^{\pm\lambda_1}_{\alpha_1b_1}e^{-\lambda_2}_{\alpha_2b_2}}{\sqrt{\bar{m}_b\bar{m}_{b_1}\bar{m}_{b_2}}}e^{\pm i\mathbf{q_1}\mathbf{r}_{l_1}}e^{-i\mathbf{q_2}\mathbf{r}_{l_2}}, \tag{S.7}$$

$$V_{\pm\pm}^{(4)}=\sum_{b,l_1b_1,l_2b_2,l_3b_3}\sum_{\alpha\alpha_1\alpha_2\alpha_3}\Phi^{\alpha\alpha_1\alpha_2\alpha_3}_{0b,l_1b_1,l_2b_2,l_3b_3}\frac{e^{\lambda}_{\alpha b}e^{\pm\lambda_1}_{\alpha_1b_1}e^{\pm\lambda_2}_{\alpha_2b_2}e^{-\lambda_3}_{\alpha_3b_3}}{\sqrt{\bar{m}_b\bar{m}_{b_1}\bar{m}_{b_2}\bar{m}_{b_3}}}e^{\pm i\mathbf{q_1}\cdot\mathbf{r}_{l_1}}e^{\pm i\mathbf{q_2}\cdot\mathbf{r}_{l_2}}e^{-i\mathbf{q_3}\cdot\mathbf{r}_{l_3}}. \tag{S.8}$$

$N_{\mathbf{q}}$ is the total number of $\mathbf{q}$ points. $\mathbf{R}$ is a reciprocal lattice vector. The Kronecker deltas $\Delta_{\mathbf{q}+\mathbf{q}_1+\mathbf{q}_2,\mathbf{R}}$ and $\Delta_{\mathbf{q}+\mathbf{q}_1+\mathbf{q}_2+\mathbf{q}_3,\mathbf{R}}$ describe the momentum selection rule and have the property that $\Delta_{m,n}=1$ (if $m=n$), or 0 (if $m\neq n$). $\Phi^{\alpha\alpha_1\alpha_2}_{0b,l_1b_1,l_2b_2}$ and $\Phi^{\alpha\alpha_1\alpha_2\alpha_3}_{0b,l_1b_1,l_2b_2,l_3b_3}$ are the third- and fourth-order force constants, which are calculated from DFT to the 5th and 2nd nearest neighbor by Quantum Espresso[2], respectively. e is the phonon eigenvector. $\bar{m}_b$ is the average

atomic mass at the lattice site b. The delta function $\delta(\Delta\omega)$ in the calculation of each $\mathcal{L}$ is evaluated by the Lorentzian function $\frac{1}{\pi}\frac{\epsilon}{(\Delta\omega)^2+\epsilon^2}$.

The thermal conductivity within the relaxation time approximation (RTA) including both three-phonon and four-phonon scattering is:

$$\kappa_{3+4,\mathrm{RTA},z} = \frac{1}{V}\sum_{\lambda} v_{z,\lambda}^2 c_\lambda (\tau_{3,\lambda,\mathrm{RTA}}^{-1} + \tau_{4,\lambda,\mathrm{RTA}}^{-1})^{-1}. \tag{S.9}$$

Here λ stands for the phonon mode $(\mathbf{q}, j)$ with j labeling the phonon dispersion branch. V is crystal volume, v_z is phonon group velocity projection along the transport direction z, and c_λ is phonon specific heat per mode.

Iterative Scheme: Exact solution to linearized BTE.

For the systems in which the Normal processes dominate over Umklapp processes, an iterative scheme that exactly solve the BTE beyond RTA needs to be employed. The relaxation time τ_λ of mode λ is obtained as

$$\tau_\lambda = \tau_{\lambda,\mathrm{RTA}}(1+\Theta_\lambda), \tag{S.10}$$

with

$$1/\tau_{\lambda,\mathrm{RTA}} = \tau_{3,\lambda,\mathrm{RTA}}^{-1} + 1/\tau_{4,\lambda,\mathrm{RTA}}^{-1} + \sum_{\lambda'\neq\lambda}\Gamma_{\lambda\lambda'}^{\mathrm{iso}}, \tag{S.11}$$

$$\Theta_\lambda = \sum_{\lambda'\lambda''}^{(+)}\Gamma_{\lambda\lambda'\lambda''}^{+}(\xi_{\lambda\lambda''}\tau_{\lambda''} - \xi_{\lambda\lambda'}\tau_{\lambda'}) + \sum_{\lambda'\lambda''}^{(-)}\frac{1}{2}\Gamma_{\lambda\lambda'\lambda''}^{-}(\xi_{\lambda\lambda''}\tau_{\lambda''} + \xi_{\lambda\lambda'}\tau_{\lambda'}) + \sum_{\lambda'\neq\lambda}\Gamma_{\lambda\lambda'}^{\mathrm{iso}}\xi_{\lambda\lambda'}\tau_{\lambda'}, \tag{S.12}$$

where $\xi_{\lambda\lambda'} = v_{\lambda',z}\omega_{\lambda'}/v_{\lambda,z}\omega_\lambda$, v_z is phonon group velocity component along the transport direction. Equation (S.10) is solved iteratively because both the left and the right hand sides contain the unknown variable τ_λ, and thus the method is called Iterative Scheme. From second-order perturbation theory [3,4], the scattering rate by the isotopes [5] is given by

$$\Gamma_{\lambda\lambda'}^{\mathrm{iso}} = \frac{\pi}{2N_c}\omega_\lambda\omega_{\lambda'}\sum_{b}^{n} g_b|\mathbf{e}_\lambda^b\cdot\mathbf{e}_{\lambda'}^{b*}|^2\delta(\omega_\lambda-\omega_{\lambda'}), \tag{S.13}$$

where

$$g_b = \sum_i f_{ib}(1-m_{ib}/\bar{m}_b)^2 \tag{S.14}$$

characterizes the magnitude of mass disorder, where i indicates isotope types, f_{ib} is the fraction of isotope i in lattice sites of basis atom b, m_{ib} is the mass of isotope i, $\bar{m}_b$ is the average atom mass of basis b sites.

Computational challenge

The large phase space of four-phonon processes and the large dimension of the fourth order force constant have made the computation extremely challenging. The computational cost

of four-phonon scattering is roughly $\sim 10^7$ times of the three-phonon scattering calculation without special techniques in our cases. To make the calculation practical without losing accuracy, we have mitigated the computational cost as described in our previous work[1]. Even after the mitigation, the computational cost is still 7,000 times of the three-phonon scattering calculation.

Role of Normal and Umklapp processes

It is instructive to discuss the RTA thermal conductivities for isotoptically pure materials to isolate the impact of four-phonon scattering to the intrinsic resistance and examine the sensitivity of k to the broadening parameters. As expected, the $\kappa_{3,\mathrm{RTA}}$ and $\kappa_{3+4,\mathrm{RTA}}$ agree well at low temperature, while deviations of these occur at high temperature and increase linearly with temperature as seen in Fig. S3. The broadening factors from the lower bound (0.05 THz) to the upper bound (0.25 THz) in calculating the four-phonon scattering rates give little variation in κ for all temperatures. Our $\kappa_{3,\mathrm{RTA}}$ of silicon is also compared to the calculated results in the literature [6,7] as well as those by ourselves via different DFT packages [8,9] to validate its reliability.

The difference between iterative and RTA thermal conductivities comes from subtle differences in Normal and Umklapp processes. Umklapp processes provide thermal resistance, degradation of a flowing distribution of phonons. Normal processes do not degrade the overall current but play the important role of redistributing thermal energy amongst the various modes in the system. If Normal processes dominate over Umklapp processes, the RTA solution does not accurately represent κ as it treats Normal processes as purely resistive and underestimates κ[10]. We find that three-phonon scattering is dominated by Normal processes in diamond and BAs, not so in Si, as seen in Fig. S4. Thus, diamond and BAs require an exact solution for three-phonon scattering[10]. As for four-phonon scattering, we find that Umklapp processes strongly dominate over Normal processes for all three materials. Thus treating the four-phonon scattering at the RTA level within the iteration scheme is likely a good approximation.

Translational invariance and interatomic truncation

Numerical uncertainties lead to small violations in crystal invariance constraints that can lead to significant deviations in calculated κ [11]. Translational invariance (TI) is thus enforced for all sets of force constants, 2^{nd}, 3^{rd} and 4^{th} order. In the calculation of scattering matrix, the truncation of IFCs may significantly reduce the computational cost, but it can break the enforced TI to some extent. We find that a small break of TI, e.g., the truncation at 3rd-IFCs<0.001 eV/Å^3 and 4th-IFCs<0.1 eV/Å^4, can only affect the low frequency scattering rates by overestimating them, while other higher frequency phonons are little affected. Examples of the four-phonon scattering for Si and BAs are shown in Fig. S5. The truncation of IFCs breaks the TI conditions and consequently deviates from the law: $\lim_{\omega\to 0}\tau^{-1} = 0$. The impacts on higher energy phonons and the overall thermal conductivity are small. In the results presented in this paper, we strictly enforce the TI

conditions and include all the IFCs values without truncation to ensure the accuracy of prediction.

Broadening factors, q-meshes and force constant cutoff radius

The convergence issue is critical for phonon scattering and thermal conductivity calculations. The four-phonon scattering calculation has been examined towards different broadening factors and **q**-meshes to ensure its accuracy. The results are in consistency for all the cases as seen in Fig. S6. Also, we have checked the convergence towards the 4th order force constant cutoff radius. In contrast to three-phonon scattering which does not converge until the 5th nearest neighbor, we find that the four-phonon scattering rates converge at the 2nd nearest neighbor. When the cutoff radius of fourth order force constants increases from the 2nd to the 3rd nearest neighbors, only the very-low-energy phonons' four-phonon scattering rates are slightly affected while all the others remain the same. The change of thermal conductivity is less than 1%.

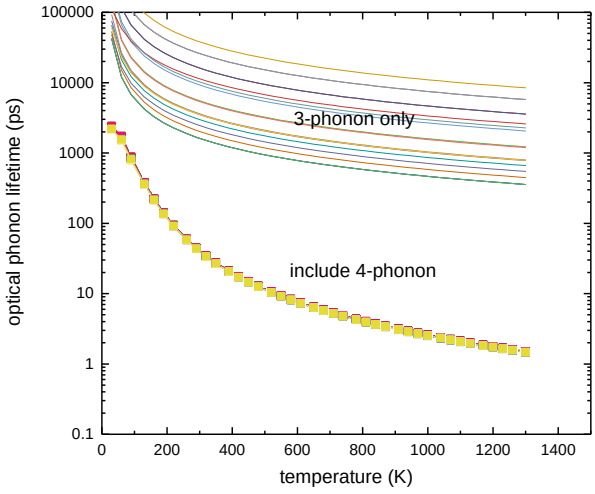

FIG. S1: **Optical phonon lifetime near the Γ point as a function of temperature of BAs.**

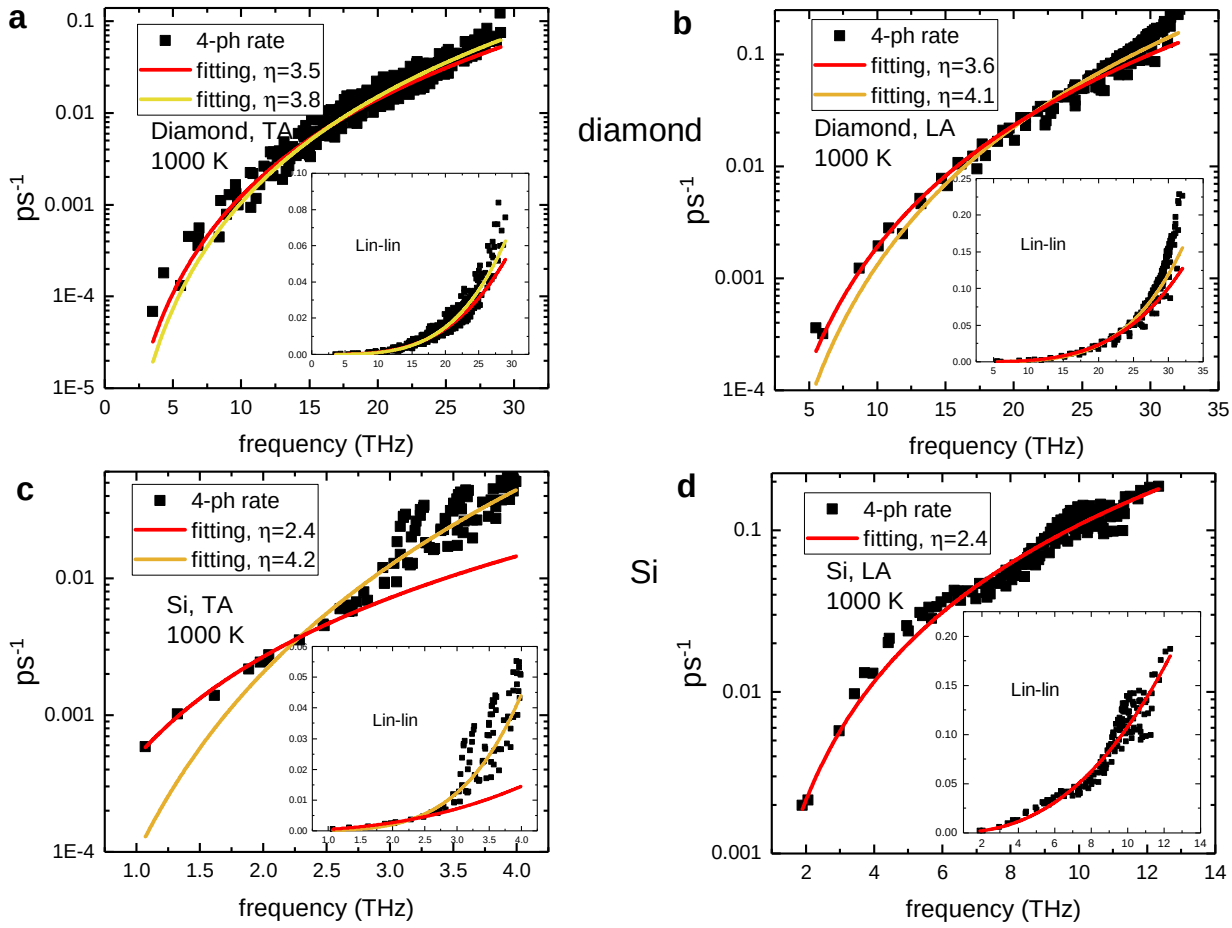

FIG. S2: **Power law fitting $\tau_4^{-1} = A\omega^\eta$ of the acoustic phonons in diamond and Si**. Each panel is plotted in log-linear scale to give a clear view of the low frequency behavior, while the inset is in linear-linear scale for a clearer view of the high frequency behavior. **a** and **b** are the TA and LA modes of diamond at 1000 K, respectively. **c** and **d** are the TA and LA modes of Si at 1000 K, respectively. We note that four-phonon scattering is only important for diamond and Si at higher temperatures. For each of **a**, **b** and **c**, we have two fitting curves: the red one (lower power) fits better the low frequency behavior, while the yellow curve (higher power) fits better in the higher frequency range.

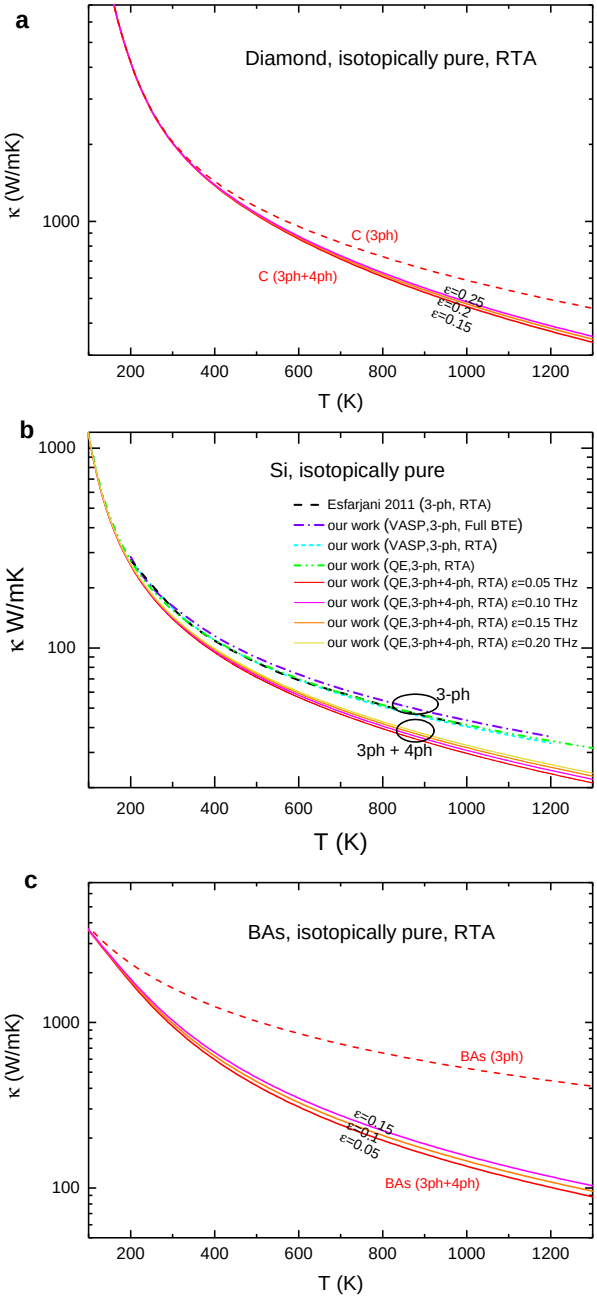

FIG. S3: **RTA thermal conductivities of isotopically pure materials calculated using different broadening factors.**

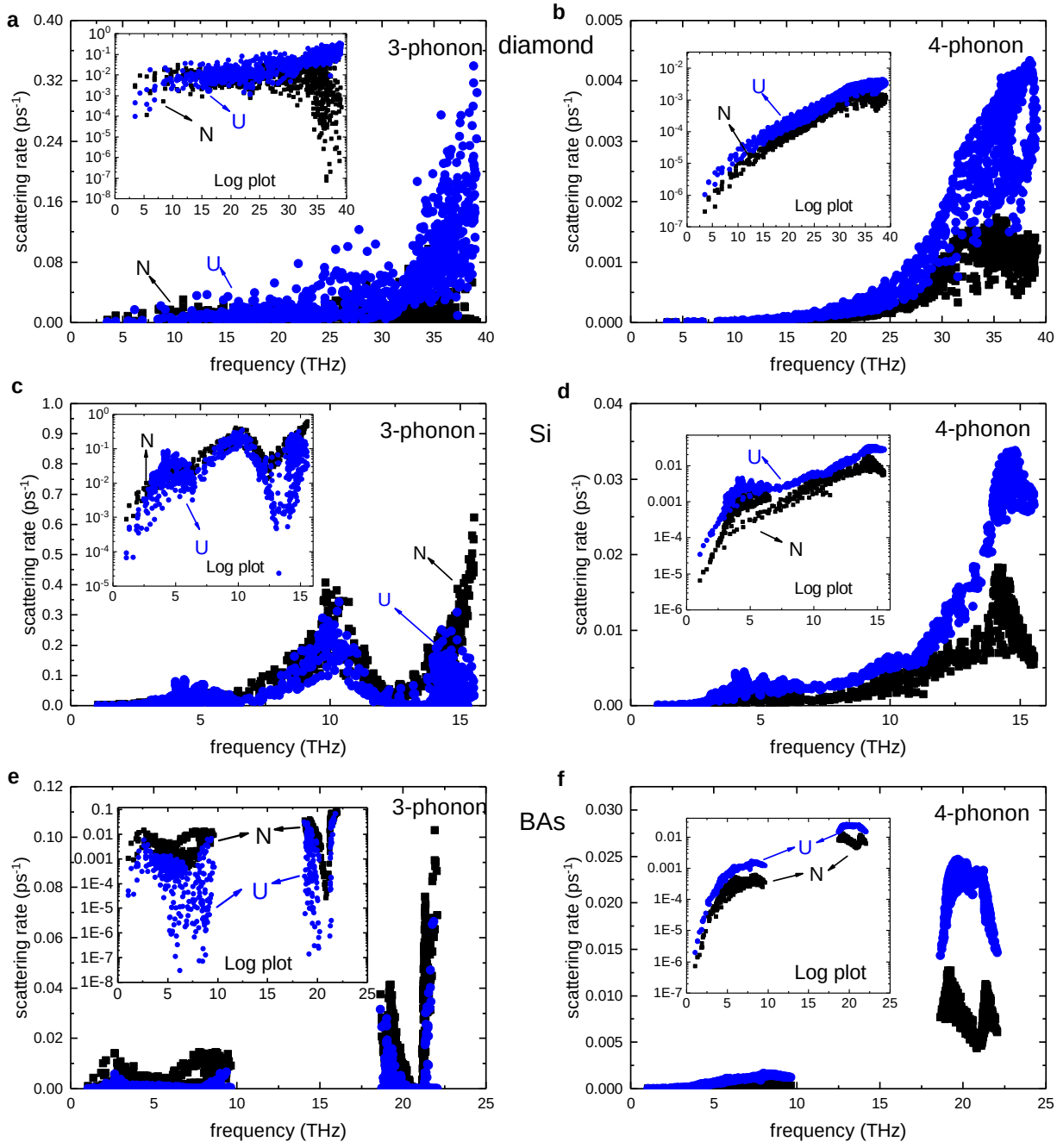

FIG. S4: Comparison between Normal and Umklapp scattering rates for diamond, Si and BAs at T=300K. Each panel is plotted in linear-linear scale, while each inset is in log-linear scale.

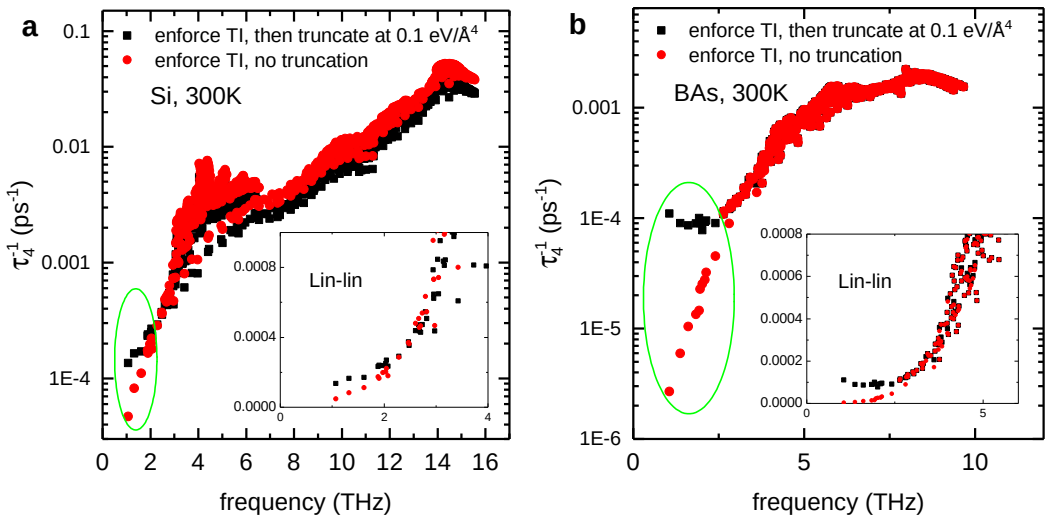

FIG. S5: Four-phonon scattering rates calculated from the IFCs with/without truncations. The truncation of IFCs affects the low-energy behavior.

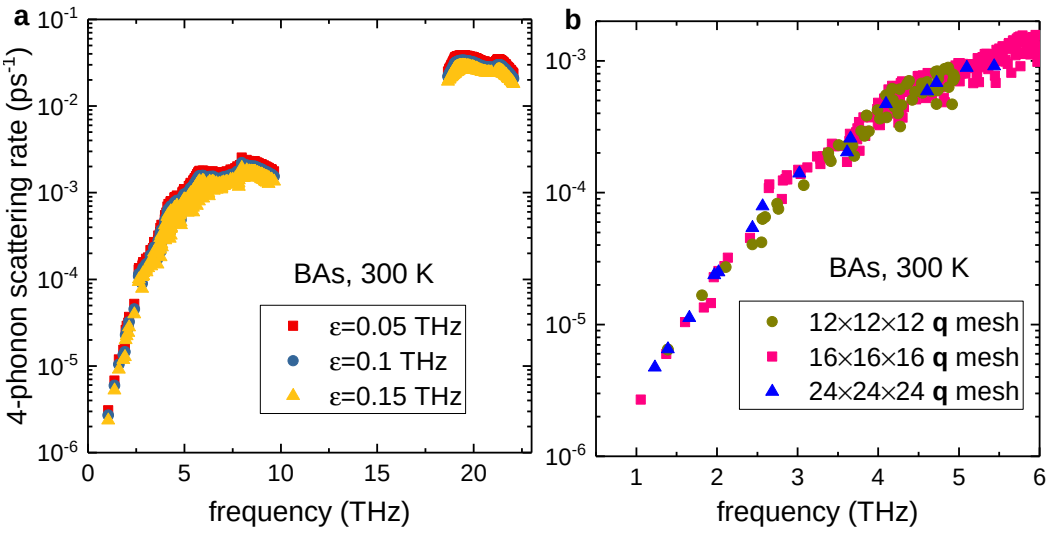

FIG. S6: Four-phonon scattering rates calculated using different broadening factors and **q**-meshes.

* Electronic address: ruan@purdue.edu

[1] T. Feng and X. Ruan, Physical Review B **93**, 045202 (2016), ISSN 2469-9950, URL http://link.aps.org/doi/10.1103/PhysRevB.93.045202.

[2] P. Giannozzi, S. Baroni, N. Bonini, M. Calandra, R. Car, C. Cavazzoni, D. Ceresoli, G. L. Chiarotti, M. Cococcioni, I. Dabo, et al., Journal of physics: Condensed matter **21**, 395502 (2009).

[3] P. Klemens, *Solid State Physics*, vol. 7 (Academic Press Inc., New York, USA, 1958).

[4] J. M. Ziman, *Electrons and Phonons* (Oxford University Press, London, 1960).

[5] S.-i. Tamura, Physical Review B **27**, 858 (1983), URL http://journals.aps.org/prb/abstract/10.1103/PhysRevB.27.858.

[6] K. Esfarjani, G. Chen, and H. T. Stokes, Physical Review B **84**, 085204 (2011), ISSN 1098-0121, URL http://link.aps.org/doi/10.1103/PhysRevB.84.085204.

[7] A. Jain and A. J. McGaughey, Computational Materials Science **110**, 115 (2015), ISSN 09270256, URL http://www.sciencedirect.com/science/article/pii/S092702561500511X.

[8] G. Kresse, Phys. Rev. B **54**, 169 (1996).

[9] W. Li, J. Carrete, N. a. Katcho, and N. Mingo, Computer Physics Communications **185**, 1747 (2014), ISSN 00104655.

[10] D. A. Broido, M. Malorny, G. Birner, N. Mingo, and D. A. Stewart, Applied Physics Letters **91**, 231922 (2007), ISSN 00036951, URL http://aip.scitation.org/doi/10.1063/1.2822891.

[11] L. Lindsay, D. a. Broido, and T. L. Reinecke, Physical Review B **87**, 165201 (2013), ISSN 1098-0121, URL http://link.aps.org/doi/10.1103/PhysRevB.87.165201.